AIP | Applied Physics Letters

Characterization of density-of-states and parasitic resistance in a-InGaZnO thin-film transistors after negative bias stress

Chunhyung Jo, Sungwoo Jun, Woojoon Kim, Inseok Hur, Hagyoul Bae et al.

Citation: Appl. Phys. Lett. **102**, 143502 (2013); doi: 10.1063/1.4800172
View online: http://dx.doi.org/10.1063/1.4800172
View Table of Contents: http://apl.aip.org/resource/1/APPLAB/v102/i14
Published by the American Institute of Physics.

Characterization of density-of-states and parasitic resistance in a-InGaZnO thin-film transistors after negative bias stress

Chunhyung Jo, Sungwoo Jun, Woojoon Kim, Inseok Hur, Hagyoul Bae, Sung-Jin Choi, Dae Hwan Kim, and Dong Myong Kim[a)]
School of Electrical Engineering, Kookmin University, Jeongneung-dong, Seongbuk-gu, Seoul 136-702, South Korea

(Received 19 December 2012; accepted 21 March 2013; published online 9 April 2013)

Instability mechanism of amorphous InGaZnO thin-film transistors under negative bias stress (NBS) was investigated. After strong NBS stress, we observed a negligible change in the subthreshold swing which is strongly dependent on the subgap density-of-states (DOS). On the other hand, there was substantial increase in the drain current at above-threshold operation. Therefore, the dominant mechanism of the NBS-induced instability is investigated not to be a change in the subgap DOS but a change in the parasitic resistance caused by the reduced Schottky barrier of the metal contacts. This was verified by the extracted source/drain resistance and Technology Computer-Aided Design simulation. © *2013 American Institute of Physics*. [http://dx.doi.org/10.1063/1.4800172]

Amorphous indium-gallium-zinc-oxide (a-IGZO)-based thin-film transistors (TFTs) have attracted much attention for flexible displays due to possible fabrication at a low temperature with high uniformity over large area at low cost.[1,2] In real display operation, TFTs are most of the time subjected to a negative gate bias stress, which maintains the "off" state of the pixel. Thus, characterization of physical mechanisms on bias/current/temperature/illumination induced instabilities is recognized as a key issue for mass production.[3] The subgap density-of-states (DOS) over the forbidden bandgap of the *a*-IGZO film is one of the most important parameters determining both electrical performance and reliability characteristics. There have been many reports on the extraction of the subgap DOS in a-IGZO TFTs by using C-V characteristics,[4,5] the conductance measured at low temperature,[6] the Meyrer-Neldel rule of the activation energy (E_A),[7] a numerical simulation-based fitting,[8] and the differential ideality factor technique.[9] For characterization of the negative bias stress (NBS) effects, previous works mainly focused on the variation of the subgap DOS in the active channel region which is fully depleted during the NBS stress.[10,11]

In this work, the instability mechanism of a-IGZO TFTs under NBS was systematically investigated. In particular, we considered a variation of the source/drain resistance ($R_{SD} = R_S + R_D$) caused by the degradation of the Schottky barrier at the source/drain contacts as well as the change of the subgap DOS. Moreover, the NBS effect was examined by experimental measurement and Technology Computer-Aided Design (TCAD) simulation for the same a-IGZO TFTs under identical bias conditions.

For characterization of instability mechanisms in a-IGZO TFTs under NBS stress with the gate bias $V_G < 0$, we employed bottom gate structure with an etch stopper as shown in Fig. 1(a). TFTs have a gate insulator with an effective oxide thickness $T_{ox} = 258$ nm ($SiN_X/SiO_X = 400$ nm/50 nm), the a-IGZO film thickness $T_{IGZO} = 45$ nm, the channel width/length $W/L = 50\ \mu m/25\ \mu m$, and the gate-to-S/D overlap $L_{ov} = 13\ \mu m$. Negative bias stress at $V_{GS/D} = -10$ V, -20 V, and -30 V with a common source/drain ($V_{DS} = 0$) was applied at room temperature (RT). For comparative analysis, characteristic parameters are focused on the threshold voltage (V_T), the on-current (I_{on} at $V_{GS/D} = 20$ V, $V_{DS} = 0.1$ V), the subthreshold slope (SS), parasitic source/drain resistance (R_{SD}), and the subgab ($E_V < E < E_C$) DOS ($g_A(E)$). The channel resistance method (CRM)[12] and the differential ideality factor technique (DIFT)[9] were employed for characterization of R_{SD} and $g_A(E)$.

I_D-V_{GS} characteristics of a-IGZO TFTs before and after NBS stress with $V_{GS/D} = -10$, -20, and -30 V at RT are shown in Fig. 1(b). Compared to the initial state before exposing to NBS, I_{on} in the linear region increases with the stress time under a large negative bias. On the other hand, as clearly shown in the semi-log plot of the transfer characteristics, we experimentally observed no shift of the threshold voltage and no change in the SS even after severe bias condition of the NBS for 20 000 s at $V_{GS/D} = -30$ V. We note, in particular, that the NBS-induced increase of I_{on} is more significant at a large negative bias stress. I_D-V_{DS} characteristics before and after NBS stress are compared in Fig. 2(a). Compared to the initial state before exposing to NBS, the drain current I_D increases with increasing the stress time (t_{NBS}) under a large negative bias.

In the first, for a possible mechanism in NBS-exposed a-IGZO TFTs, we investigated t_{NBS}-dependent change in the subgap DOS. $g_A(E)$ can be obtained by the DIFT,[8] through the subthreshold drain current $I_{D,sub}$ and subthreshold slope SS as

$$I_{D,sub} \cong I_{Do} \exp\left(\frac{V_{GS} - V_T}{\eta(V_{GS})V_{th}}\right), \quad SS = 2.3\eta(V_{GS})V_{th}\ for\ V_{GS} < V_T, \tag{1}$$

$$\eta(V_{GS}) = 1 + \frac{C_{DOS}(V_{GS})}{C_{ox}}, \tag{2}$$

[a)]Author to whom correspondence should be addressed. Electronic mail: dmkim@kookmin.ac.kr. Tel.: +82-2-910-4719. Fax: +82-2-910-4449.

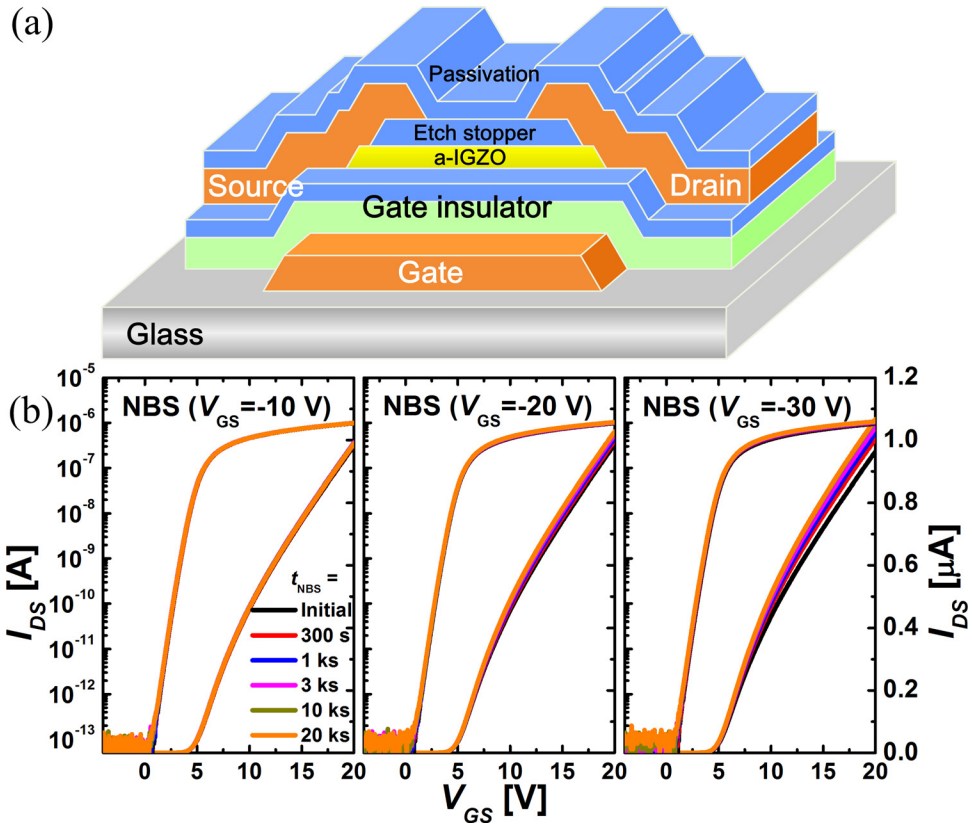

FIG. 1. (a) Schematic view of the a-IGZO with an inverted staggered bottom-gate structure. (b) NBS time evolution (under $V_{GS/D} = -10$ V, -20 V, and -30 V at RT without illumination) of the transfer curve characteristics.

$$C_{DOS}(V_{GS}) = \int_{\psi_S(V_{GS}=V_{FB})}^{\psi_S(V_{GS})} C_{ox}\left(\frac{d\eta(V_{GS})}{dV_{GS}} \Big/ \frac{d\psi_S}{dV_{GS}}\right) d\psi_S, \quad (3)$$

$$g_A(E) = \frac{\Delta C_{DOS}(V_{GS})}{q^2 T_{IGZO}} \ [\mathrm{eV}^{-1}\mathrm{cm}^{-3}]. \quad (4)$$

The t_{NBS}-dependent $g_A(E)$ is extracted by using the DIFT as plotted in Fig. 3. Extracted $g_A(E)$ can be decomposed into a superposition of deep and tail states in exponential forms as

$$g_A(E) = N_{DA}\exp(E - E_C/kT_{DA}) + N_{TA}\exp(E - E_C/kT_{TA}). \quad (5)$$

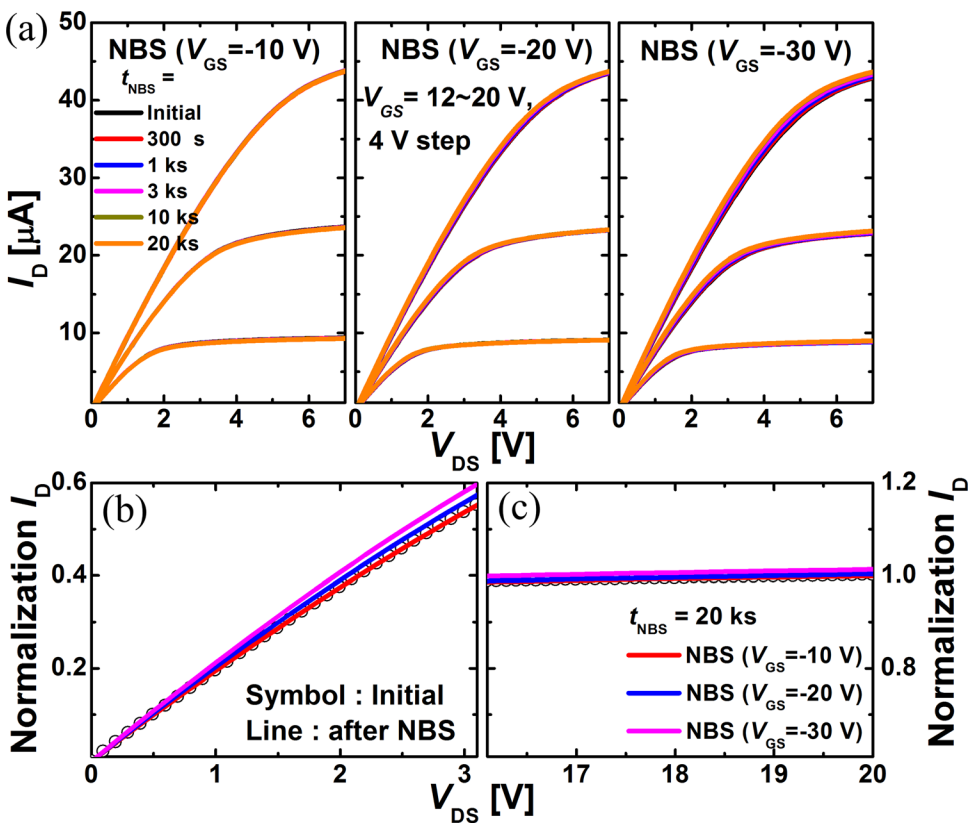

FIG. 2. (a) I_D-V_{DS} characteristics for the NBS at $V_{GS/D} = -10$ V, -20 V, and -30 V. Normalized I_D-V_{DS} characteristics (b) linear region and (c) saturation region.

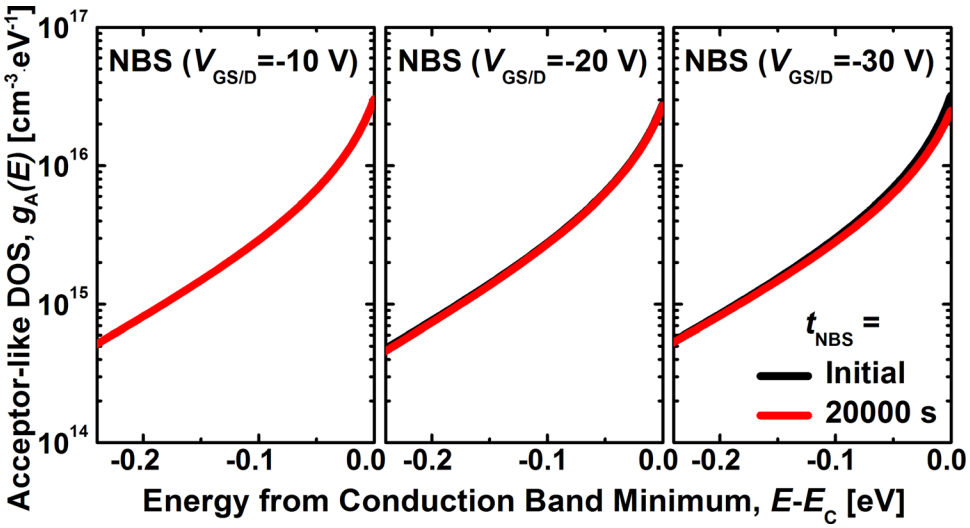

FIG. 3. Subgap DOS ($g_A(E)$) extracted from the measured I_D-V_{GS} characteristics through the DIFT before and after NBS tests for 20 000 s.

We confirmed that $g_A(E)$ in the active channel region was independent of t_{NBS} under NBS stress for $V_{GS/D} = -10$, -20, and -30 V as shown in Fig. 3. This is because the electric field under NBS stress is confined only to the overlapped region of the gate metal with the S/D contacts. There is very small vertical field in the active channel region, and therefore the NBS causes no stress on the active region of the channel. Therefore, a negligible change is observed in DOS under NBS stress.

In the second, the parasitic resistance effect is characterized through the I-V characteristics of a-IGZO TFTs under above-threshold bias with $V_{GS} > V_T$. The property of contacts on the active a-IGZO layer depends on the Schottky barrier, due to the inherent property of a-IGZO TFTs, the voltage drop across the parasitic resistances should be considered in the modeling and characterization.[13,14] Considering the voltage drop across the parasitic resistances, the drain current in the linear mode with small drain bias ($V_{DS} \ll V_{GS} - V_T$) is described by

$$I_D \cong 2K\{(V_{GS,ext} - I_D R_S - V_T) \times [V_{DS,ext} - I_D(R_S + R_D)]\}, \quad (6)$$

with $K \equiv (\mu C_{ox} W/2L)$, μ the channel carrier mobility, and C_{ox} the effective gate capacitance per unit area (F/cm^2). We

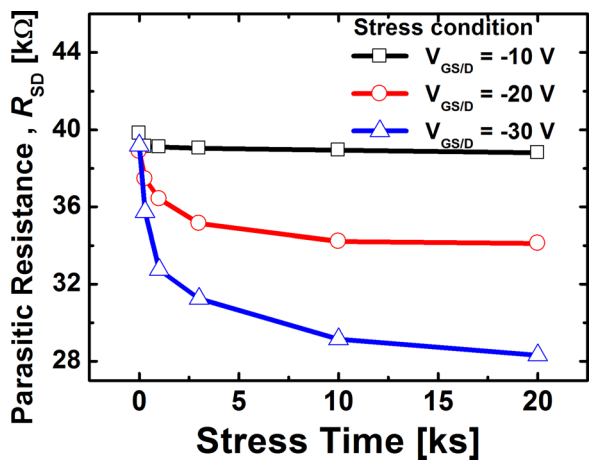

FIG. 4. (a) NBS time evolution ($V_{GS/D} = -10$, -20, and -30 V) of the parasitic resistance.

note that there are parasitic source (R_S) and drain resistances (R_D). They are strongly dependent on the process condition, source/drain metals, and the doping and composition of the active layer. In particular, the parasitic resistances are mainly caused by the Schottky-like non-ideal Ohmic contacts at the source and drain on the a-IGZO active layer.

As shown in the NBS stress dependence of the normalized I_D in Figs. 2(b) and 2(c), there is considerable change in the I_D-V_{DS} and I_D-V_{GS} characteristics, especially under a large gate voltage. This observation of increasing drain current after large NBS stress is expected to be caused by the change in R_S and R_D rather than the change in the subgap DOS in the active region. Under a large NBS stress, there is no conducting path over the active region. Therefore, there is a negligible vertical field across the a-IGZO active region, and this causes no influence on the active layer. On the other hand, there is a strong vertical field across the overlapped region of the gate metal with the S/D contacts on the edge of the channel region. This may cause a considerable effect on the contact property of the S/D metal on the active layer. This causes a significant change in the S/D contact resistance by the modification of the Schottky barrier. This suggests that charge trapping at the metal-semiconductor interface is dominant mechanism for Schottky barrier instability. As shown in the above equations, the drain current can be increased without change of V_T, if the effective gate voltage ($V_{GS} = V_{GS,ext} - I_D R_S$) or the effective drain voltage ($V_{DS} = V_{DS,ext} - I_D(R_S + R_D)$) is increased due to reduced R_S and R_D after NBS stress.

R_{SD} (obtained from the CRM through $R_{SD} = V_{DS}/I_D|V_{GS} \gg V_T$) is expected to be mainly for the contact resistance at the source and drain (R_S, R_D). R_{SD} is extracted to decrease by $\Delta R_{SD} = 10.9\,k\Omega$ (from 39.2 to 28.3 kΩ) after $t_{NBS} = 20\,000$ s under NBS at $V_{GS/D} = -30$ V as shown in Fig. 4. A cross-sectional illustration under NBS stress is shown in Fig. 5(a) for a TCAD verification of the electric field distribution under NBS stress. As shown in Fig. 5(b) for the simulation results, we clearly observed that the electric field is confined to the overlapped region while the electric field in the active channel region with a floated back surface is almost unchanged under NBS stress whatever the gate bias is $V_G = -30$ V or $V_G = -10$ V. However, the electric fields

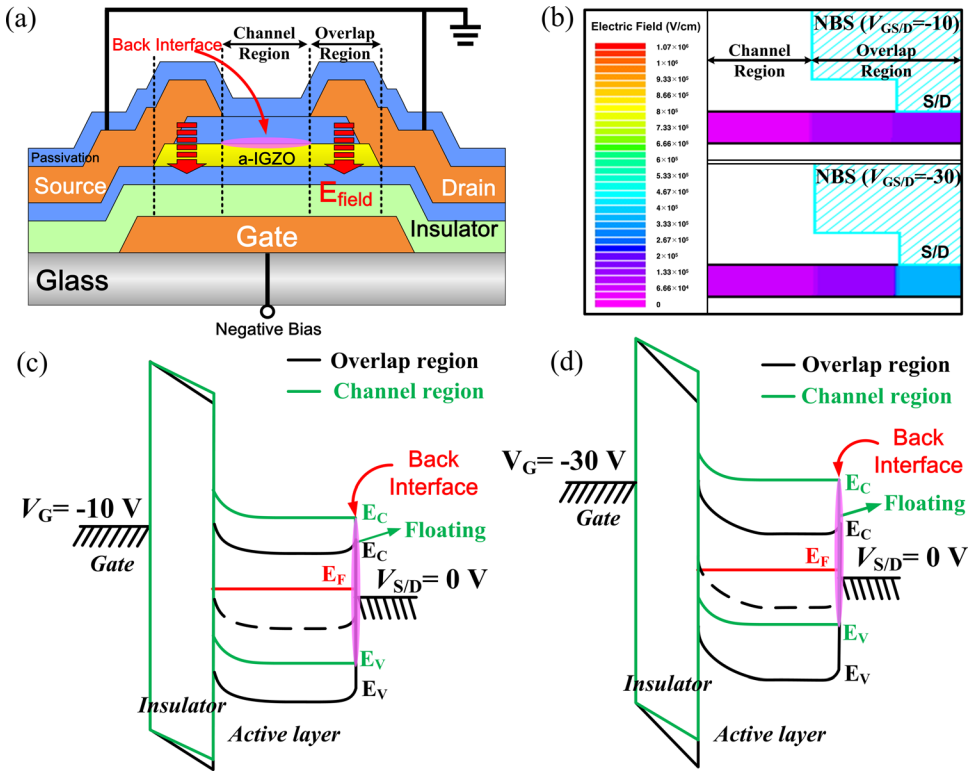

FIG. 5. (a) A cross-sectional field distribution of a-IGZO TFTs under NBS. (b) TCAD simulation result. Energy band diagrams under NBS (c) at $V_{GS/D} = -10$ V (d) at $V_{GS/D} = -30$ V. High field is formed at the overlap region.

TABLE I. Extracted acceptor-like DOS and parasitic resistance in a-IGZO TFTs after NBS ($V_{GS/D} = -10$, -20, and -30 V).

		Acceptor-like DOS				
Stress condition	t_{NBS} [s]	N_{TA} [$cm^{-3}\,eV^{-1}$]	kT_{TA} [eV]	N_{TD}[$cm^{-3}\,eV^{-1}$]	kT_{TD} [eV]	R_{SD} [kΩ]
$V_{G,S/D} = -10$ V	Initial	1.97×10^{16}	0.016	9.16×10^{15}	0.084	**39.8**
	20 000	1.97×10^{16}	0.016	9.16×10^{15}	0.084	**38.7**
$V_{G,S/D} = -20$ V	Initial	1.92×10^{16}	0.016	9.39×10^{15}	0.082	**38.8**
	20 000	1.92×10^{16}	0.016	9.39×10^{15}	0.081	**34.4**
$V_{G,S/D} = -30$ V	Initial	2.20×10^{16}	0.016	9.21×10^{15}	0.087	**39.2**
	20 000	2.07×10^{16}	0.016	9.16×10^{15}	0.087	**28.3**

right above the gate metal and right below the S/D contact at the overlapped region are very strong as shown in Figs. 5(c) and 5(d).

Extracted $g_A(E)$ and R_{SD} are summarized in Table I. The parasitic resistance change ΔR_{SD} caused by the NBS at $V_{GS/D} = -30$ V is larger than that under $V_{GS/D} = -10$ V while a negligible change in $g_A(E)$ for both cases.

We investigated the physical mechanisms of the NBS time evolution of a-IGZO TFTs. We observed that there is negligible change in the subgap DOS for the active region while a considerable change in the parasitic resistance. This is characterized to be a Schottky barrier change due to a large electric field across the S/D metal to the gate overlapped region. On the other hand, there is negligible change in the subgap DOS over the active channel region. This is due to a small electric field over the channel region with floated back channel region even under a large NBS stress. This doesn't put any stress over the active channel under NBS stress for the accumulation mode n-channel a-IGZO TFTs. Therefore, the dominant mechanism under the NBS stress is expected to be a reduction of the parasitic resistance caused by the Schottky barrier reduction with a negligible change in the subgap DOS.

This work was supported by the National Research Foundation of Korea (NRF) grant funded by the Korea government (Grant Nos. 2010-0013883 and 2012-0000147). The CAD software was supported by SILVACO and IC Design Education Center (IDEC).

[1]K. Nomura, H. Ohta, A. Takagi, T. Kanmiya, M. Hirano, and H. Hosono, Nature (London) **432**, 488 (2004).
[2]M. K. Kim, J. H. Jeong, H. J. Lee, T. K. Ahn, H. S. Shin, J. S. Park, J. K. Jeong, Y. G. Mo, and H. D. Kim, Appl. Phys. Lett. **90**, 212114 (2007).
[3]T. Kamiya, K. Nomura, and H. Hosono, Sci. Technol. Adv. Mater. **11**, 044305 (2010).
[4]M. Kimura, T. Nakanishi, K. Nomura, T. Kamiya, and H. Hosono, Appl. Phys. Lett. **92**, 133512 (2008).
[5]S. Lee, S. Park, S. Kim, Y. Jeon, K. Jeon, J.-H. Park, J. Park, I. Song, C. J. Kim, Y. Park, D. M. Kim, and D. H. Kim, IEEE Electron Device Lett. **31**, 231 (2010).
[6]S. Lee and A. Nathan, Appl. Phys. Lett. **101**, 113502 (2012).
[7]C. Chen, K. Abe, H. Kumomi, and J. Kanicki, IEEE Trans. Electron Device **56**, 1177 (2009).

[8]H.-H. Hsieh, T. Kamiya, K. Nomura, H. Hosono, and C.-C. Wu, Appl. Phys. Lett. **92**, 133503 (2008).
[9]M. Bae, D. Yun, Y. Kim, D. Kong, H. K. Jeong, W. Kim, J. Kim, I. Hur, D. H. Kim, and D. M. Kim, IEEE Electron Device Lett. **33**, 399 (2012).
[10]Y.-G. Chang, T.-W. Moon, D.-H. Kim, H. S. Lee, J. H. Kim, K.-S. Park, C.-D. Kim, and S. Im, IEEE Electron Device Lett. **32**, 1704 (2011).
[11]T. C. Chen, T. C. Chang, T. Y. Heieh, W. S. Lu, F. Y. Jian, C. T. Tsai, S. Y. Huang, and C. S. Lin, Appl. Phys. Lett. **99**, 022104 (2011).
[12]H. Bae, S. Kim, M. Bae, J. S. Shin, D. Kong, H. Jung, J. Jang, J. Lee, D. H. Kim, and D. M. Kim, IEEE Electron Device Lett. **32**, 761 (2011).
[13]S. Lee, J.-H. Park, K. Jeon, S. Kim, Y. Jeon, D. H. Kim, D. M. Kim, J. C. Park, and C. J. Kim, Appl. Phys. Lett. **96**, 113506 (2010).
[14]B.-Y. Tsui, C.-P. Lu, and H.-H. Liu, IEEE Electron Device Lett. **29**, 1053 (2008).